RSC Advances

PAPER

View Article Online
View Journal | View Issue

Cite this: *RSC Adv.*, 2020, **10**, 44034

Construction of magnetic $MgFe_2O_4$/CdS/MoS_2 ternary nanocomposite supported on NaY zeolite and highly efficient sonocatalytic degradation of organic pollutants†

Meysam Sadeghi, Saeed Farhadi * and Abedin Zabardasti

In this work, the novel magnetically separable NaY zeolite/$MgFe_2O_4$/CdS nanorods/MoS_2 nanoflowers nanocomposite was successfully synthesized through the ultrasonic-assisted solvothermal approach. FESEM, EDAX, XRD, FTIR, TEM, AFM, VSM, N_2-BET, UV-vis DRS and PL were utilized to identify the as-synthesized nanocomposite. Subsequently, the sonocatalytic activity of this nanocomposite was assessed in the degradation of organic dyes, including methylene blue (MB), rhodamine B (RhB) and methyl orange (MO) from water solutions for the first time. Several analytical parameters like irradiation time, process type, initial MB concentration, H_2O_2 concentration, catalyst dosage, organic dye type, and US power have been systematically investigated to attain the maximum sonocatalytic yield. Regarding the acquired data, the NaY/$MgFe_2O_4$/CdS NRs/MoS_2 NFs sonocatalyst was incredibly able to completely eliminate the MB *via* engaging the US/H_2O_2 system. The kinetic evaluates demonstrated the sonodegradation reactions of the MB followed a first-order model. The apparent rate constant (k_{app}) and half-life time ($t_{1/2}$) acquired for the sonodegradation process of MB utilizing the US/H_2O_2/NaY/$MgFe_2O_4$/CdS NRs/MoS_2 NFs system were measured to be 1.162 min and 0.596 min^{-1}, respectively. The free $^{\bullet}OH$ radicals were also recognized as the main reactive oxygen species in the MB sonodegradation process under US irradiation. In addition, the outcomes of the recyclability study of the NaY/$MgFe_2O_4$/CdS NRs/MoS_2 NFs sonocatalytic clearly displayed a less than 6% drop of the catalytic activity in up to four sequential runs. Lastly, a plausible mechanism for the sonodegradation reaction of organic dyes was suggested and discussed.

Received 16th October 2020
Accepted 1st December 2020

DOI: 10.1039/d0ra08831e

rsc.li/rsc-advances

1. Introduction

Today, due to the rapid development of worldwide industrialization, environmental contamination has become a catastrophic issue concerning much attention around the globe. The evacuation of very high quantities of toxic effluents from different industries into the environment causes dire consequences to public human health and aquatic ecosystems.[1,2] Meanwhile, textile and dyeing effluents from synthetic organic dyes are considered as the main source of water contamination.[3,4] Annually, about 2.5×10^5 tons (~15%) of hazardous organic dyes are discarded into the effluents during textile dyeing operations.[5] On the other hand, these compounds due to their aromatic structures are resistant to elimination through biodegradation methods.[4] Hence, these types of pollutants must be wholly eliminated from effluents before their disposal into the environment. Until now, multiple different methodologies have been investigated for the effective removal of organic dyes from effluents, including electrochemical treatment, coagulation–flocculation, membrane filtration, adsorption, sonodegradation and photodegradation processes, and more.[6]

Among various methods, the sonolysis process has been applied as a remarkable and environmentally friendly route with high performance to remove organic dyes through the free $^{\bullet}OH$ radicals as well as the other reactive oxygen species (ROPs) like H_2O, $^{\bullet}O_2H$ radicals and so on.[7] Additionally, it has been considered that the use of various semiconductor sonocatalysts along with the ultrasonic (US) irradiation can in turn lead to the decrease of the reaction time duration and subsequently the increase of degradation efficiency compared with the US system alone.[8] Regarding the above discussion, a series of semiconductor sonocatalysts, including MIL-101(Cr),[2] TiO_2,[9] $MnFe_2O_4$,[10] $LuFeO_3$,[11] CdS,[12] Cu_2S,[13] CuO,[14] $MnFe_2O_4$/MIL-101(Cr),[10] ZnO/GR/TiO_2,[15] CuS/$CoFe_2O_4$,[6] CdSe/GQDs,[16] Cu: ZnS-NPs-AC,[17] TiO_2/AC,[18] $InVO_4$/TiO_2 (ref. [19]) and other have been investigated to eliminate the organic pollutants *via* the US process. Nonetheless, it is a necessity to design and develop

Department of Chemistry, Lorestan University, Khorramabad 68151-433, Iran. E-mail: farhadi.s@lu.ac.ir; Fax: +98 66 33120618; Tel: +98 66 33120611

† Electronic supplementary information (ESI) available. See DOI: 10.1039/d0ra08831e

a novel magnetically separable sonocatalytic system that can lead to more effective eliminate the organic pollutants from aqueous solutions.

In recent years, cadmium sulfide (CdS) as an n-type semiconductor[20–22] has spurred remarkable attention due to their different applications, including solar cells, photocatalysis, photoluminescence and electroluminescence, photovoltaic and electrical performances.[22–24] Plus, several considerable properties of the CdS such as simple fabrication, special physical and chemical structure, and high stability, make it a proper candidate for water treatment operations.[4] For this purpose, the CdS can be utilized as a sonocatalyst for the degradation of organic chemical contaminants from effluents. Nevertheless, due to the narrow band gap energy ~2.4 eV, the rapid recombination of excited h^+–e^- pairs as well as low quantum efficiency, the practical application of the CdS is remarkably decreased.[4] In order to solve these limitations, the CdS can be combined with other semiconductors to promote its sonocatalytic performance.

In the past few decades, molybdenum disulfide (MoS_2) as an p-type semiconductor with a band gap energy approximately 1.9 eV (ref. [25]) has been investigated as a suitable material owing to its unique properties like low toxicity, high catalytic performance, thermal and chemical stability, and high absorption capacity. In this regard, MoS_2 has been widely applied in multiple applications such as super capacitors, sensors, Li-ion batteries, photocatalysts and more.[25–29] Hence, MoS_2 is introduced as a competitive candidate for hybridizing with the CdS by the production of p–n heterojunction system to prevent the h^+–e^- pairs recombination and improve the sonocatalytic activity. On the other hand, because recycling is an imperative factor in developing a particular sonocatalyst, we utilized a magnetic material to make the nanocomposite. Currently, the spinel ferrites nanostructures have received a lot of attention because of their outstanding features compare with those of the balk structures.[30] Among all types of spinel ferrites known so far, magnesium ferrite nanoparticles ($MgFe_2O_4$ NPs) semiconductor with band gap energy of 1.5–2.4 eV (ref. [31]) illustrate excellent supermagnetic features. For this reason, they can be utilized in various fields such as catalysis,[31–33] adsorption,[34–36] sensor,[37] drug delivery,[38] *etc.* Besides, coupling the MoS_2/CdS with the $MgFe_2O_4$ purveys a promising heterojunction system for improving the catalytic activity and recycling *via* using a simple external magnetic field.

Furthermore, the high surface area and adsorbent capacity are two important factors that help to enhance the sonocalytic process yield. As NaY zeolite displays advantageous properties like extensive pore volume, high surface area, excellent adsorption capacity, biocompatibility and remarkable hydrothermal constancy, it has been designated for diverse applications in multiple fields for instance in the adsorbents synthesis and catalysis.[39–43] In this respect, the NaY zeolite was selected as suitable supports to enhance the overall sonocatalytic process efficiency, because it acts as an excellent electron acceptor–donor and transporter.

Based on the aforementioned considerations, in the current work, the novel magnetically separable NaY zeolite/$MgFe_2O_4$/CdS nanorods/MoS_2 nanoflowers nanocomposite was synthesized *via* the ultrasonic-assisted solvothermal method and subsequently its catalytic performance was investigated to degrade the three organic dyes from water solutions by engaging the hydrogen peroxide (H_2O_2) as a source of free $^{\bullet}OH$ radicals under US irradiation. Regarding the determined band gap energies and reactive oxidative species during the sonodegradation test, a plausible mechanism was suggested and discussed. However, to our knowledge, no previous research has yielded on the sonocatalytic degradation of organic dyes using the NaY zeolite/$MgFe_2O_4$/CdS NRs/MoS_2 NFs nanocomposite.

2. Experimental

2.1. Materials

All the chemicals required in this study were directly of analytical grade and utilized with high purity. Sodium silicate (Na_2SiO_3), sodium hydroxide (NaOH), aluminum hydroxide ($Al(OH)_3$), iron nitrate nonahydrate ($Fe(NO_3)_3\cdot 9H_2O$), cadmium nitrate tetrahydrate ($Cd(NO_3)_2\cdot 4H_2O$), magnesium nitrate hexahydrate ($Mg(NO_3)_2\cdot 6H_2O$), ethylenediamine (EDA), disodium ethylenediaminetetraacetate (EDTA), *tert*-butyl alcohol (*t*-BuOH), thiourea (TU), hexaammonium heptamolybdate tetrahydrate ($(NH_4)_6Mo_7O_{24}\cdot 4H_2O$), benzoquinone (BQ), methylene blue (MB), rhodamine B (RhB), and methyl orange (MO) were gained from Sigma-Aldrich and Merck companies.

2.2. Characterization

In order to obtain the structural, morphological, magnetic and optical features of the as-prepared sonocatalysts, several different analyses were applied. The particles size and morphology of the samples surface were gathered using the field emission scanning electron microscopy (MIRA3 TESCAN) accompanied with the dispersive X-ray spectroscopy (FESEM-EDAX) analysis. The functional groups of the sonocatalysts were investigated by the Fourier transform infrared (FTIR) analysis on a spectrophotometer (Shimadzu system FTIR 160) applying KBr pellets in the wavelength range of 400–4000 cm^{-1}. To precisely characterize the morphology and particle size of the achieved samples, the transmission electron microscopy (TEM) analysis was utilized on an electron microscope (Philips CM120) at voltage of 80 kV. As well, *via* using the vibrating sample magnetometer (VSM, Magnetic Daghigh Kavir, MDKB model), the magnetic features were evaluated. The X-ray diffraction (XRD) analysis of the catalysts were identified *via* a STOE diffractometer applying Ni-filtered CuKα ($\lambda = 1.54$ Å) radiation under 40 mA/40 kV on a scanning speed of 2° min^{-1} within the 2θ region of 5° to 80°. The atomic force microscope (AFM) was also taken on a noncontact mode, Ara-AFM, Iran, model Full plus to attain the surface topology and particle size of the catalysts. To detailed explore the pore size distribution and specific surface area, the nitrogen Brunauer–Emmett–Teller (N_2-BET) analysis was carried out on a PHSCHINA PHS1020 device at 77 K. A UV-vis diffuse reflectance spectra (DRS) instrument was utilized to investigate the optical absorption properties on a spectrophotometer (Scinco S4100) by the

standard of $BaSO_4$ in the wavelength range of 250–800 nm. Furthermore, the sonodegradation reactions of organic dyes were implemented by using a sonoreactor (UP100H) with an frequency of 30 kHz and the acoustic power of 100 W. Additionally, in order to monitor the absorption spectra of the organic dyes during the sonodegradation processes, the ultraviolet-visible (UV-vis) spectrophotometer (Cary 100, Varian Company) was applied in the wavelength range of 200–800 nm. The photoluminescence (PL) analysis of the as-fabricated catalysts was done utilizing a fluorescence spectrophotometer (F-4500, Hitachi) under an excitation wavelength of 330 nm.

2.3. Synthesis of $MgFe_2O_4$ NPs

The $MgFe_2O_4$ NPs were fabricated utilizing the hydrothermal method. In this respect, the amounts of 1.57 g of $Fe(NO_3)_3 \cdot 9H_2O$ and 0.5 g of $Mg(NO_3)_2 \cdot 6H_2O$ were introduced into 30 mL of deionized water and stirred continuously for 1 h to get a clear solution. Next, 0.5 mol L^{-1} of NaOH solution was slowly added into the as-prepared suspension to gain the pH 8 and stirred for another 1 h. The achieved mixture was subsequently placed into a Teflon-lined stainless steel autoclave to be treated hydrothermally at 180 °C for 12 h. Consequently, the resulting precipitate was thoroughly rinsed using deionized water and ethanol solvents for several times and dried at 70 °C for 10 h.

2.4. Synthesis of NaY zeolite

To 4.9 g of $Al(OH)_3$ and 5 g of NaOH, 10 mL of deionized water was added and subsequently stirred to obtain a clear solution. The as-prepared solution was then heated at 100 °C. In the next step, 5 g of the as-achieved suspension was appended into 2.95 g of NaOH and 30.5 mL of deionized water and re-stirred for 1 h (solution labelled A). Simultaneously, 11 g of Na_2SiO_3 gently added into 30.5 mL of deionized water and 2.95 g of NaOH and stirred for 1 h (solution labeled B). Afterwards, the solution A was slowly mixed with solution B and the attained mixture was stirred for 40 min. The mixture was then put into a Teflon-lined stainless steel autoclave and left to be heated at 90 °C for 8 h. The resulting precipitate was filtered and thoroughly washed *via* deionized water for multiple times to gain a pH $\sim$ 7 and eventually held at 100 °C.

2.5. Synthesis of MoS_2 NFs

The hydrothermal route was used to attain the MoS_2 nanoflowers as follows: briefly, the values of 0.2 g of $(NH_4)_6Mo_7O_{24} \cdot 4H_2O$ and 1.28 g of TU were poured into 40 mL of deionized water and subsequently stirred vigorously for 30 min. After stirring, the as-obtained solution was introduced into a Teflon-lined stainless steel autoclave and treated *via* the heat at 200 °C for 24 h. Afterwards, the resulting precipitate was washed utilizing deionized water and ethanol for several times and finally dried at 80 °C for 12 h.

2.6. Synthesis of NaY/$MgFe_2O_4$/CdS NRs/MoS_2 NFs

The NaY/$MgFe_2O_4$/CdS NRs/MoS_2 NFs nanocomposite was synthesized using an ultrasonic-assisted solvothermal strategy. Firstly, 0.15 g of each previously fabricated $MgFe_2O_4$, MoS_2 and NaY and 40 mL of EDA were added into 20 mL of deionized water and sonicated for 1 h. After sonication, the values of 0.64 g of $Cd(NO_3)_2 \cdot 4H_2O$ and 0.32 g of TU were appended into the above suspension and sonicated for 30 min. The mixture was then moved into a Teflon-lined stainless steel autoclave and heated at 160 °C for 24 h. Afterwards, the resulting precipitate was filtered and washed utilizing ethanol and deionized water for five times and consequently dried at 80 °C for 12 h. In addition to this, bare CdS, NaY/$MgFe_2O_4$, $MgFe_2O_4$/CdS NRs and NaY/CdS NRs/MoS_2 NFs sonocatalysts were successfully synthesized for the sonodegradation studies of organic dyes.

2.7. Sonocatalytic experiments

The sonocatalytic performance of the as-obtained NaY zeolite/$MgFe_2O_4$/CdS NRs/MoS_2 NFs nanocomposite was investigated using the sonodegradation of MB, RhB and MO dyes in the presence of ultrasonic irradiation. In brief, 10 mg of NaY/$MgFe_2O_4$/CdS NRs/MoS_2 NFs catalyst was poured into 50 mL of 25 mg L^{-1} of MB solution. In the next step, the as-achieved suspension was agitated magnetically in darkroom for 30 min. Upon producing an adsorption–desorption equilibrium between the dye molecules and NaY/$MgFe_2O_4$/CdS NRs/MoS_2 NFs surface, the aliquot of 2 mL of H_2O_2 (4 mM) was added to the above suspension and exposed under ultrasonic irradiation. Then, every 30 seconds, about 2 mL of this suspension was magnetically separated using an external magnetic field to completely eliminate the suspended sonocatalyst from the reaction reservoir. Eventually, the sonodegradation reaction was monitored through the MB absorption peak at $\lambda_{max} \sim$ 663 nm utilizing the UV-vis absorption spectrophotometer device. It is to be noted that the temperature of system was kept constant at 25 $\pm$ 2 °C *via* using the circulating water. In addition, the effects of different analytical parameters affecting on the sonodegradation reactions of organic dyes like irradiation time (0.5, 1, 1.5, 2, 2.5, 3, 3.5, 4, 4.5 and 5 min), H_2O_2 concentration (1, 2, 3, 4 and 5 mM), sonocatalyst dosage (5, 10, 25, 50, 75 and 100 mg), initial dye concentration (25, 35 and 45 mg L^{-1}), and sonocatalyst type (bare CdS, bare MoS_2, bare $MgFe_2O_4$, $MgFe_2O_4$/CdS, NaY/$MgFe_2O_4$, and NaY/CdS/MoS_2) were checked in detail. Moreover, the sonodegradation process efficiency% outlined by applying the equation in below (1):

$$\text{Efficiency}\% = \left[\frac{C_0 - C_t}{C_0}\right] \times 100 \quad (1)$$

In the presented equation, C_0 and C_t factors display the dye concentration at the initial solution and the desired irradiation time (as per mg L^{-1}), respectively.

3. Result and discussion

3.1. FESEM analysis

The morphology and particle size of the bare NaY zeolite (Fig. 1a and b), NaY/$MgFe_2O_4$ (Fig. 1c and d), NaY/$MgFe_2O_4$/CdS NRs/MoS_2 NFs (Fig. 1e and f), bare MoS_2 NFs (Fig. 1g and h), bare

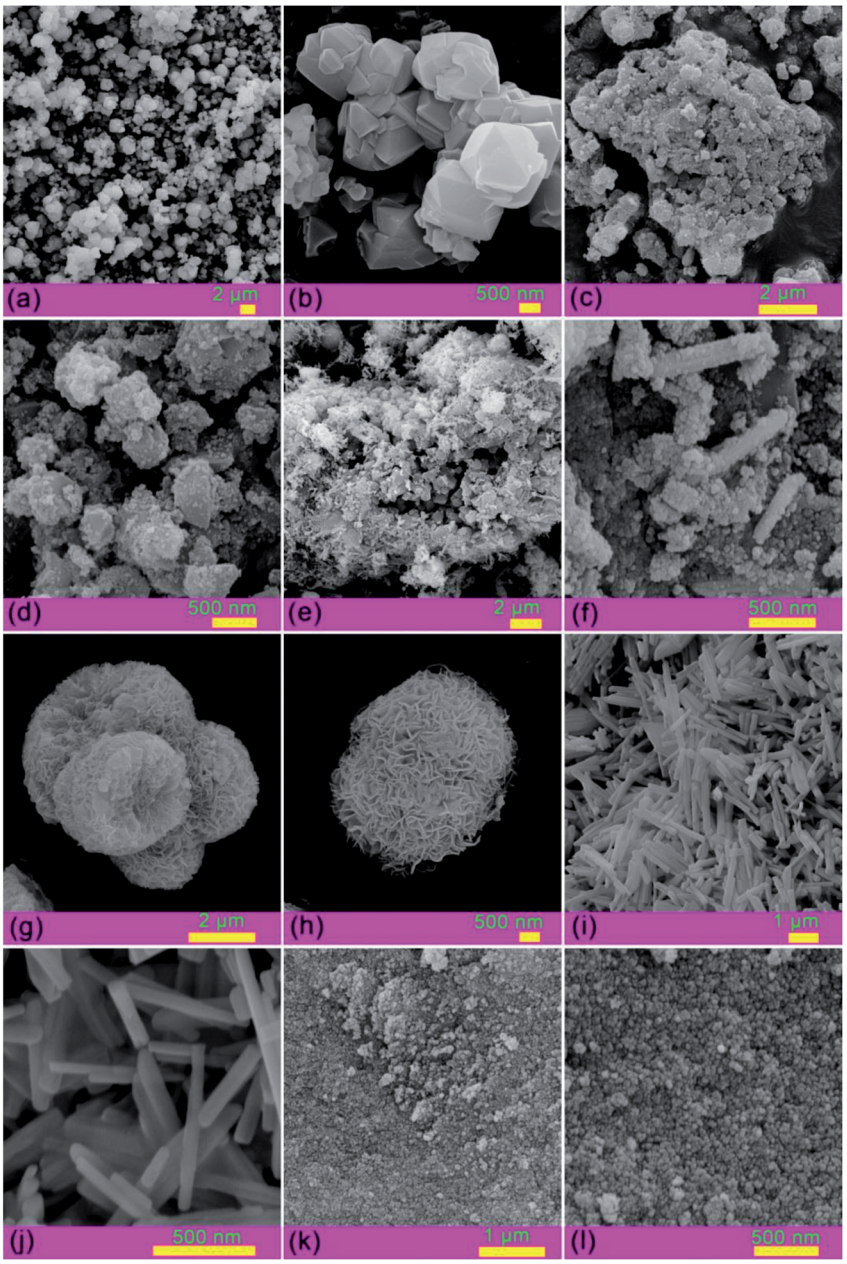

Fig. 1 FESEM images of: (a) and (b) bare NaY, (c) and (d) NaY/$MgFe_2O_4$, (e) and (f) NaY/$MgFe_2O_4$/CdS/MoS_2, (g) and (h) bare CdS, (i) and (j) bare MoS_2, and (k) and (l) bare $MgFe_2O_4$.

CdS NRs (Fig. 1i and j), and bare $MgFe_2O_4$ (Fig. 1k and l) were studied applying the field emission scanning electron microscopy (FESEM) analysis as represented in Fig. 1. On the basis of Fig. 1, NaY zeolite particles have an octahedral in shape with a high surface area within the range of ~1–2 μm. Based on the gained FESEM images, the sphere-like and flower in shape morphologies of $MgFe_2O_4$ NPs and MoS_2 NFs, as well as the rod in shapes of the CdS were all obviously validated. Moreover, the $MgFe_2O_4$ NPs and MoS_2 NFs with average particle size of ~15 nm and 2 μm, demonstrating in Fig. 1, are uniformly embedded on the NaY zeolite surface. In addition to this, the average diameter and length of the CdS NRs were obtained to be 65 nm and ~1, μm, respectively. As well, the FESEM images of the NaY/$MgFe_2O_4$/CdS NRs/MoS_2 NFs clearly illustrated that the morphology of this nanocomposite remain unchanged after hybridizing with the CdS NRs, MoS_2 NFs and $MgFe_2O_4$ NPs.

3.2. EDAX analysis

In order to distinguish the chemical decomposition of the as-achieved sonocatalysts, the energy dispersive X-ray (EDAX) analysis was exploited. The EDAX analysis of the bare NaY zeolite (Fig. 2a), NaY/$MgFe_2O_4$/CdS NRs/MoS_2 NFs (Fig. 2b), bare MoS_2 NFs (Fig. 2c), and bare CdS NRs (Fig. 2d) were shown in Fig. 2, respectively. The obtained information from the EDAX

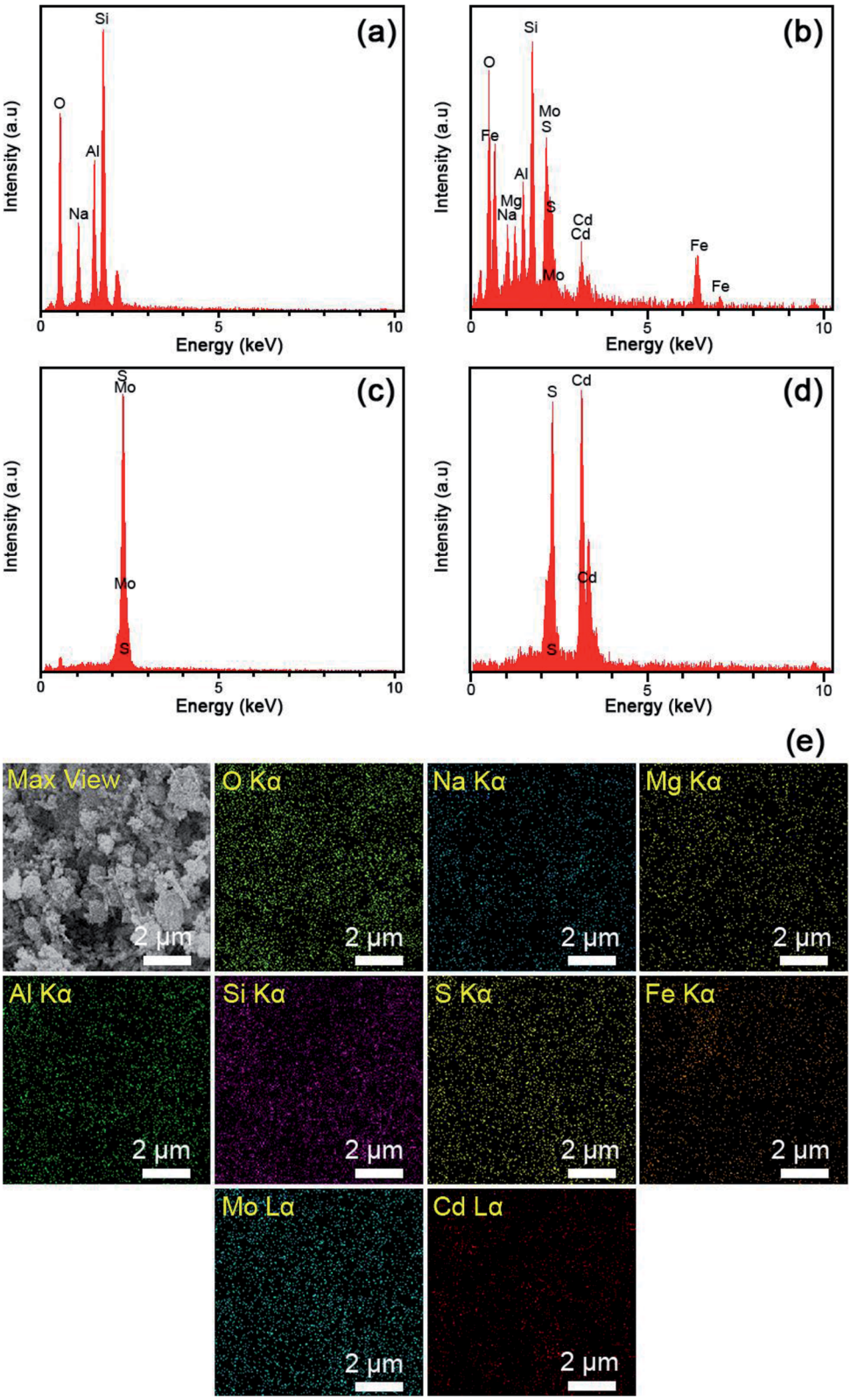

Fig. 2 EDAX analyses of: (a) bare NaY, (b) NaY/$MgFe_2O_4$/CdS/MoS_2, (c) bare MoS_2, and (d) bare CdS. (e) FESEM image along with the EDAX elemental dot-mappings of the NaY/$MgFe_2O_4$/CdS/MoS_2.

spectra are clearly interpreted to the presence of nine elements of Al, Na, Si, Cd, Mo, S, Mg, O, and Fe in the NaY/$MgFe_2O_4$/CdS NRs/MoS_2 NFs catalyst, which is in accordance with the SEM, TEM and XRD outcomes. Moreover, the atomic% and weight% of the NaY/$MgFe_2O_4$/CdS NRs/MoS_2 NFs were collected in Table S1.† Additionally, the FESEM image along with elemental

mappings of the NaY/$MgFe_2O_4$/CdS NRs/MoS_2 NFs nanocomposite were shown in Fig. 2e. According to the information illustrated in Fig. 2e, the uniform distribution of Al, Na, Si, Cd, Mo, S, Mg, O, and Fe elements in the abovementioned nanocomposite were clearly affirmed.

3.3. FTIR analysis

The Fourier transform infrared (FTIR) analysis was used to evaluate the functional groups of the as-prepared samples. Fig. 3 displays the FTIR spectra of the bare NaY zeolite (Fig. 3a), NaY/CdS NRs/MoS_2 NFs (Fig. 3b), NaY/$MgFe_2O_4$/CdS NRs/MoS_2 NFs (Fig. 3c), bare CdS NRs (Fig. 3d), and bare $MgFe_2O_4$ (Fig. 3e), respectively. As can be elucidated in Fig. 3b, seven specified bands related to the functional groups of the NaY zeolite can be observed. The two bands about 3471 cm^{-1} and 1650 cm^{-1} can be corresponded to the O–H binding and H–O–H bending vibrations of the adsorbed H_2O on the NaY zeolite surface, respectively. The absorption peak at 973 cm^{-1} is also referred to the O–T–O (T = Si and/or Al elements) external connection and internal tetrahedral asymmetrical stretching vibrations of the NaY zeolite framework. Furthermore, the two other peaks observed at 746 cm^{-1} and 667 cm^{-1} can be related to the vibrations O–T–O internal tetrahedral symmetrical stretching and external linkage, respectively. Additionally, the characteristic peaks near 561 cm^{-1} and 455 cm^{-1} respectively are allocated to the bending vibrations of the D6R external linkage and internal SiO_4^{4-} or AlO_4^{5-} tetrahedral units of the NaY zeolite. The existence of another absorption peak was detected at about 568 cm^{-1} due to the overlapping with the stretching band of the NaY zeolite at 561 cm^{-1}, which clearly affirmed the successful fabrication of the $MgFe_2O_4$ NPs on the zeolite framework. Nevertheless, upon supporting the MoS_2 NFs and CdS NRs on the surface of NaY zeolite, no specified bands were observed, revealing these nanoparticles have the Mo–S and Cd–S bonds <400 cm^{-1}. According to the FTIR spectrum in Fig. 3d, the two absorption bands of the bare $MgFe_2O_4$ were detected within the wavelength region of 400 cm^{-1} to 600 cm^{-1}, which are related to the Mg–O and Fe–O bonds, respectively. As well, the peaks at 3489 cm^{-1} and 1640 cm^{-1} were corresponded to the adsorbed water within the $MgFe_2O_4$ surface, respectively.

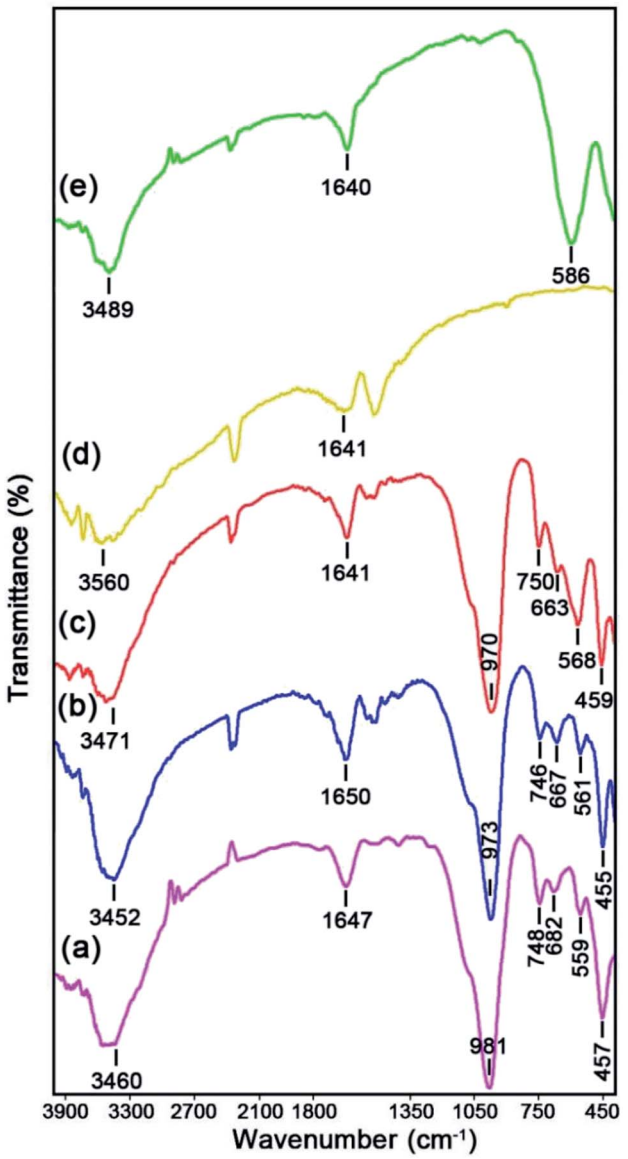

Fig. 3 FTIR spectra of: (a) bare NaY, (b) NaY/CdS/MoS_2, (c) NaY/$MgFe_2O_4$/CdS/MoS_2, (d) bare CdS NRs, and (e) bare $MgFe_2O_4$.

3.4. XRD analysis

The as-fabricated sonocatalysts well all analyzed using the X-ray diffraction (XRD) patterns to identify their crystalline and phase features as the related patterns of the bare NaY zeolite (Fig. 4a), NaY/$MgFe_2O_4$/CdS NRs/MoS_2 NFs (Fig. 4b), $MgFe_2O_4$/CdS NRs (Fig. 4c), bare MoS_2 NFs (Fig. 4d), bare CdS NRs (Fig. 4e), and bare $MgFe_2O_4$ (Fig. 4f) have been respectively illustrated in Fig. 4. Regarding the specified patterns in Fig. 4, the main narrow peaks characterized to the NaY zeolite were discerned at 2θ angles of 6.27°, 10.18°, 11.93°, 15.71°, 18.74°, 20.42°, 23.70°, 27.14°, and 32.55° respectively, which were referred to the miller indices of (111), (220), (311), (331), (511), (440), (620), (533), and (733), crystallized in the cubic structure with JCPDS no. 41-0118. Based on Fig. 4, it was found that *via* hybridizing the CdS, $MgFe_2O_4$ and MoS_2 simultaneously over the NaY zeolite to produce the NaY/$MgFe_2O_4$/CdS NRs/MoS_2 NFs nanocomposite, no remarkable change was observed within its crystalline framework. In this regard, multiple intensive peaks attributed to the CdS NRs phase used to fabricate this nanocomposite were observed at 2θ angles of 25.05°, 26.75°, 28.41°, 36.87°, 43.94°, 48.07°, 51.15°, 52.11°, 53.04°, 58.53°, 67.06°, 69.55°, 71.17°, 72.65°, and 75.74°, which were assigned to the miller indices of (100), (002), (101), (102), (110), (103), (200), (112), (201), (202), (203), (210), (211), (114), and (105) (JCPDS no. 041-1049). Moreover, several other sharp peaks were distinguished at 2θ values of 30.29°, 35.70°, 43.37°, 53.76°, 57.39°, and 62.90° respectively that are in good accordance with the (220), (311), (400), (422), (511), and (440) diffraction planes of the spinel $MgFe_2O_4$ (JCPDS no. 073-1720). Meantime, upon synthesizing the MoS_2 NFs on the surface of NaY/$MgFe_2O_4$/CdS NRs/MoS_2

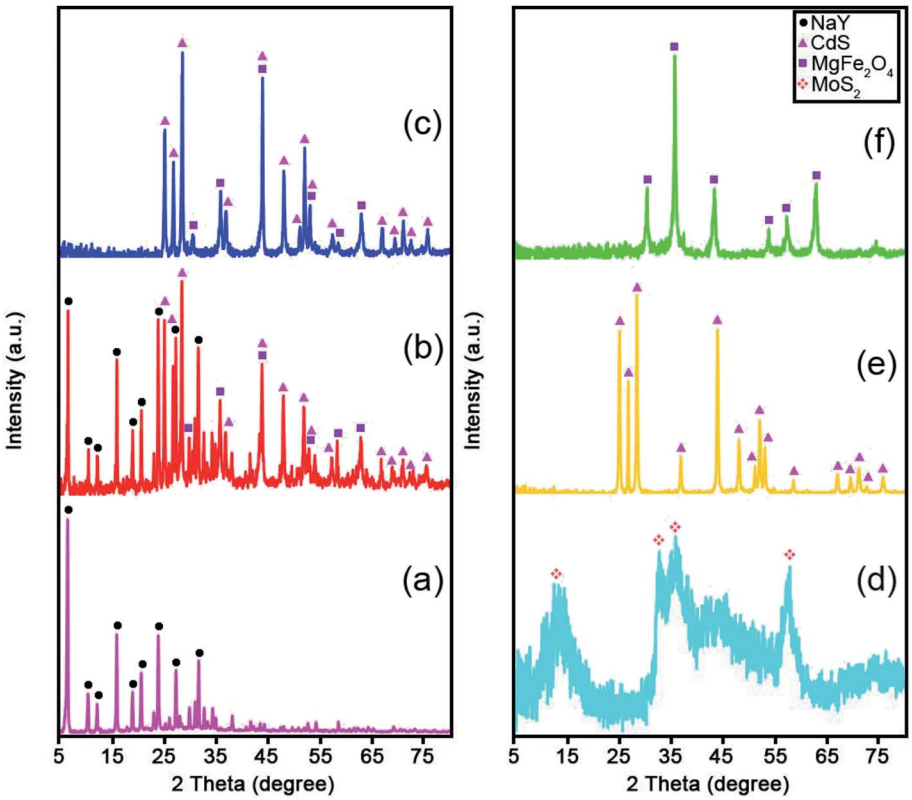

Fig. 4 XRD patterns of: (a) bare NaY, (b) NaY/$MgFe_2O_4$/CdS/MoS_2, (c) $MgFe_2O_4$/CdS, (d) bare MoS_2, (e) bare CdS NRs, and (f) bare $MgFe_2O_4$.

NFs nanocomposite, no observing peaks corresponded to the MoS_2 phase was seen, demonstrating the low crystallinity and excellent distribution of these particles in the nanocomposite framework. Additionally, as can be revealed in Fig. 4h, the prominent peaks at 2θ values of 13.12°, 32.65°, 35.81°, and 57.55° were indexed to the (002), (100), (103), and (110) diffraction planes of bare MoS_2 NFs phase (JCPDS no. 006-0097). Besides, the average particle size of the as-prepared NaY/$MgFe_2O_4$/CdS NRs/MoS_2 NFs nanocomposite was determined to be ~15 nm applying the Debye–Scherrer equation as follows (2):

$$d = 0.9\ \lambda/\beta \cos\theta \quad (2)$$

In the above equation, d and λ symbols are the average particle size and the X-ray wavelength of Ni-filtered CuKα radiation (λ = 1.54 Å) respectively, β is the full width at half maximum (FWHM) of the desired diffraction peak and the Bragg diffraction angle is defined as θ. Based on the aforementioned data, it can be understood that the enumerated catalysts, involving CdS NRs, MoS_2 NFs and $MgFe_2O_4$ NPs have been successfully fabricated on the NaY zeolite surface.

3.5. TEM analysis

In order to evaluate the particle size and morphology of the fabricated NaY/$MgFe_2O_4$/CdS NRs/MoS_2 NFs sonocatalyst, the transmission electron microscopy (TEM) analysis was performed as the obtained images are demonstrated in Fig. 5a–d at different magnifications. The TEM images of the NaY/$MgFe_2O_4$/CdS NRs/MoS_2 NFs clearly confirmed that the CdS, MoS_2 and $MgFe_2O_4$ as guest particles have been successfully immobilized within the surface of NaY zeolite. As well, the average particle size of the MoS_2 NFs and $MgFe_2O_4$ NPs were acquired to be approximately 250 nm and 15 nm, respectively. Moreover, the

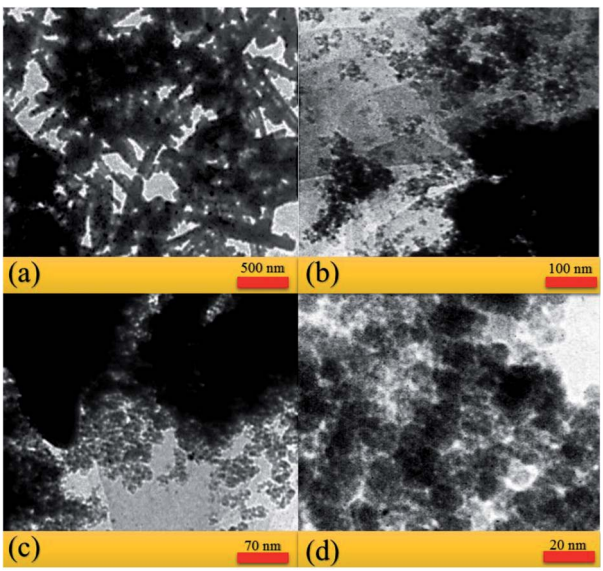

Fig. 5 TEM images of the NaY/$MgFe_2O_4$/CdS NRs/MoS_2 NFs.

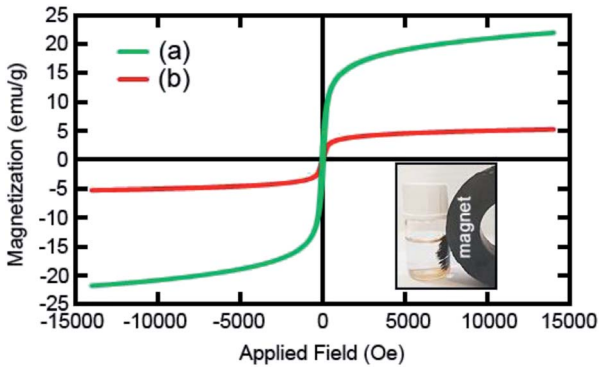

Fig. 6 VSM analysis plots of: (a) bare $MgFe_2O_4$ NPs and (b) NaY/$MgFe_2O_4$/CdS NRs/MoS_2 NFs at room temperature.

diameter and length of the CdS NRs were found to be about 60 nm and 1 μm, respectively. The abovementioned results were in good agreement with the average particle size and diameter gained by the FESEM and XRD.

3.6. VSM analysis

To fully evaluate the magnetic features of the as-prepared sonocatalysts, the vibrating sample magnetometer (VSM) analysis was carried out at room temperature *via* utilizing a magnetic field of $-14\,000 \leq Oe \leq +14\,000$. Fig. 6 elucidates the M–H plots (magnetic hysteresis loops) of the bare $MgFe_2O_4$ NPs (Fig. 6a) and NaY/$MgFe_2O_4$/CdS NRs/MoS_2 NFs (Fig. 6b). Regarding the M–H plots, the amount of saturation magnetization (M_s) for the bare $MgFe_2O_4$ NPs was gained to be approximately 21.98 emu g^{-1}, whereas after hybridizing the $MgFe_2O_4$ NPs within the NaY zeolite framework, the aforementioned amount reduced to about 5.28 emu g^{-1}, which is corresponded to the presence of nonmagnetic materials (*i.e.* CdS, MoS_2 and NaY) within the framework of nanocomposite. Furthermore, the coercive force (H_c) and remnant magnetization (M_r) amounts were approximately zero, which obviously corroborated the superparamagnetic properties of this nanocomposite. Hence, the magnetic NaY/$MgFe_2O_4$/CdS NRs/MoS_2 NFs nanocomposite catalyst can be quickly withdrawn *via* utilizing an external magnetic field from the solution reservoir after the sonodegradation reactions of the organic dyes at the desired time intervals.

3.7. BET analysis

In order to precisely obtain the structural features of the NaY zeolite/$MgFe_2O_4$/CdS NRs/MoS_2 NFs nanocomposite catalyst, the nitrogen Brunauer–Emmett–Teller (N_2-BET) analysis was employed. Fig. 7a–d reveals the N_2-BET plots of the adsorption–desorption isotherm, the pore size distribution, mesoporous volume (V_{me}), the microporous volume (V_{mi}), and the average pore diameter (nm) of the as-manufactured NaY/$MgFe_2O_4$/CdS NRs/MoS_2 NFs nanocomposite. As can be represented in Fig. 7a–d, the N_2 adsorption–desorption isotherm at 77 K displayed a type-III plot with a H3-type hysteresis loop (regarding the IUPAC classification), which obviously validates the mesoporous structure of the NaY/$MgFe_2O_4$/CdS NRs/MoS_2 NFs catalyst. Furthermore, the total pore volume, the specific surface area and the average pore diameter of this nanocomposite were determined to be 8.91 nm, 178.25 $m^2\ g^{-1}$ and 0.26 $cm^3\ g^{-1}$, respectively (see Fig. 7a and b). Additionally, by utilizing the plots of the Barrett–Joyner–Halenda (BJH) and *t*, V_{mi} and V_{me} values were acquired to be 0.24 $cm^3\ g^{-1}$ and 0.09 $cm^3\ g^{-1}$, respectively (Fig. 7c and d). Based on the abovementioned information, it can be found that the NaY zeolite/$MgFe_2O_4$/CdS

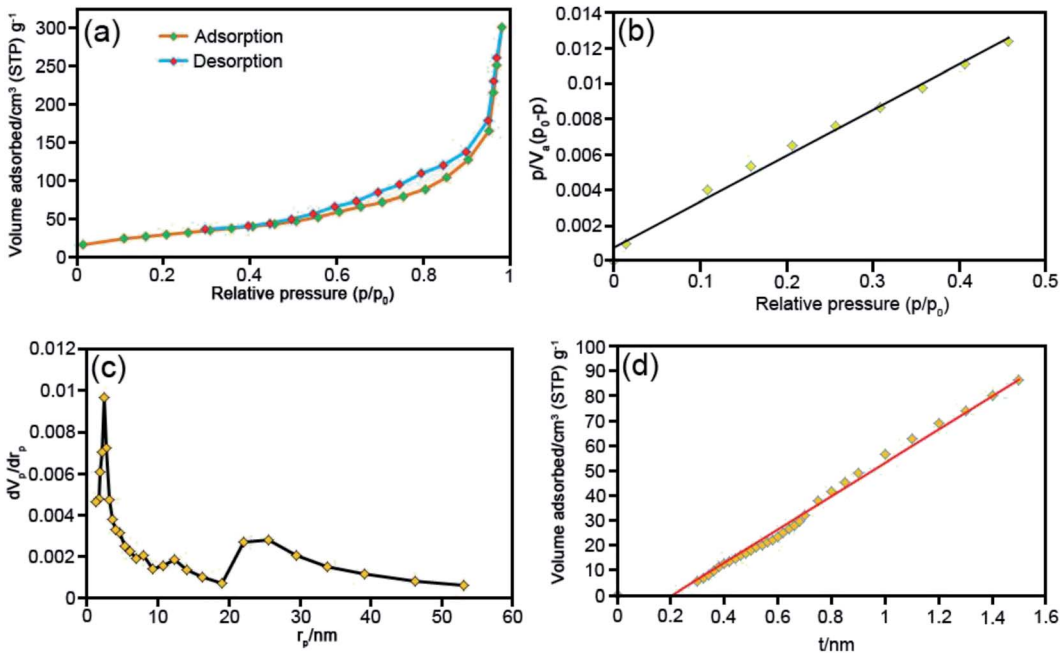

Fig. 7 (a–d) N_2-BET analyses of the NaY/$MgFe_2O_4$/CdS NRs/MoS_2 NFs.

NRs/MoS_2 NFs has the remarkable pore volumes and high specific surface area to implement the sonodegradation processes of the organic dyes.

3.8. UV-vis DRS analysis

The UV-vis diffuse reflectance spectra (DRS) measurements were implemented to investigate the optical features of the as-prepared sonocatalysts. Fig. 8a demonstrates the UV-vis DRS spectra of the bare MoS_2 NFs, bare NaY zeolite, bare CdS NRs, bare $MgFe_2O_4$ and $NaY/MgFe_2O_4/CdS\ NRs/MoS_2$ NFs. Evidently, the bare NaY zeolite does not exhibit any UV-vis absorption band at the wavelength region of 250–800 nm. Moreover, the bare CdS NRs represent strongly absorption within the UV-vis region, below a band edge approximately 540 nm, whereas the bare MoS_2 NFs show a spread absorption band in the visible light region. Additionally, the bare $MgFe_2O_4$ NPs display absorbs light at the wavelengths more than 650 nm. Meantime, upon hybridizing the MoS_2, $MgFe_2O_4$ and CdS NRs with the NaY zeolite, a broad absorption band in observed that embraced the entire visible region, illustrating a red shift compared with the CdS NRs. To precisely determine the absorption band gap energy (E_g) of the samples, Tauc's equation was used as follows (eqn (3)):

$$(\alpha h\nu)^2 = A(h\nu - E_g) \quad (3)$$

Herein α, h, ν, E_g, and A symbols are the optical absorption coefficient, Plank constant, light frequency, absorption band gape energy, as well as the constant allocated to the sonocatalysts, respectively. Fig. 8b shows the plots of $(\alpha h\nu)^2$ against $h\nu$ for the bare $MgFe_2O_4$, bare CdS NRs, bare MoS_2 NFs, and $NaY/MgFe_2O_4/CdS\ NRs/MoS_2$ NFs. The amount of $h\nu$ extrapolated to $\alpha = 0$ attains the absorption band gape energy. Regarding the spectra information, the amounts of E_g of the $MgFe_2O_4$, bare CdS NRs and bare MoS_2 NFs were calculated to be 1.64 eV, 2.4 eV, and 1.9 eV, respectively. Plus, after generation the $NaY/MgFe_2O_4/CdS\ NRs/MoS_2$ NFs quaternary nanocomposite, the E_g amount the decreased and obtained to be 2.2 eV compared with the CdS NRs, revealing the successful electronic combining the $MgFe_2O_4$, CdS NRs and MoS_2 NFs together. Thus, this fact denotes that the aforementioned nanocomposite can be used as an effective catalyst in the sonodegradation reactions of organic dyes under US irradiation.

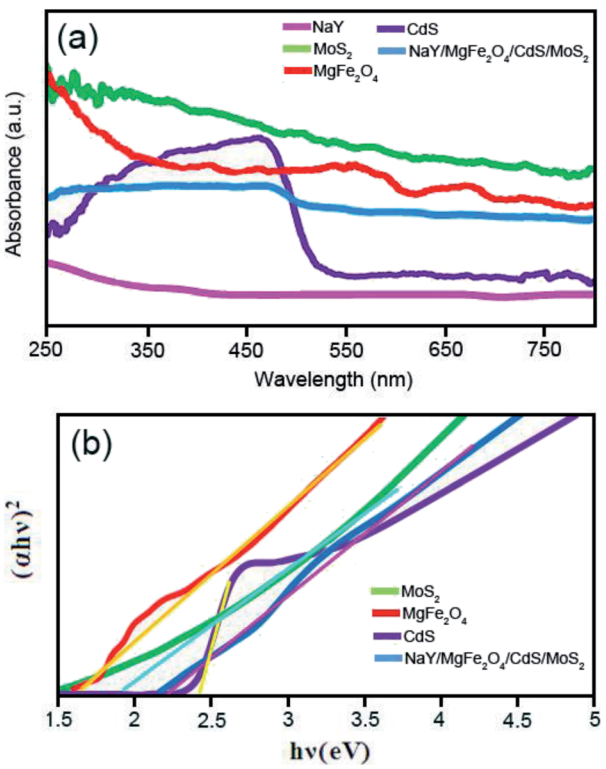

Fig. 8 (a) UV-vis DRS spectra and (b) $(\alpha h\nu)^2$–$h\nu$ plots of the as-fabricated catalysts.

3.9. Sonodegradation reaction studies

3.9.1. Effect of irradiation time. In order to determine the optimal irradiation time of the sonodegradation process of the foregoing organic dyes over the $NaY/MgFe_2O_4/CdS\ NRs/MoS_2$ NFs nanocomposite, a series of irradiation times were considered as the collected outcomes shown in Fig. 9a–c. Evaluating the gained data during the experiments obviously verified the notable relationship between the sonodegradation rate and irradiation time. Thus, the sonodegradation reactions were monitored utilizing the specified absorption peaks allocated to the MB at a λ_{max} approximately 663 nm. To this end, the optimal dosage of the $NaY/MgFe_2O_4/CdS\ NRs/MoS_2$ NFs sonocatalyst (10 mg) was firstly added into 25 mg L^{-1} of MB solution (50 mL) and the acquired suspension was exposed to the US waves in the presence of 4 mM of initial H_2O_2 concentration. From the presented UV-vis spectra in Fig. 9a, it was observed that as the reaction time goes on, the MB peak intensity ($\lambda_{max} \sim 663$ nm) gradually decreases and eventually disappears completely after 5 min. With regard to the performed experiments and the achieved findings, the noteworthy role of the $NaY/MgFe_2O_4/CdS\ NRs/MoS_2$ NFs sonocatalyst on the degradation of MB from water media obviously affirmed.

3.9.2. Sonodegradation kinetics study. In order to more precisely investigate the sonodegradation processes of organic dyes in aqueous solutions, the first-order kinetic model was also applied *via* the following eqn (4):

$$\ln(C_0/C_t) = k_{app}t \quad (4)$$

Regarding the aforementioned equation, k_{app} symbol is corresponded to the apparent reaction rate constant, C_0 is the initial concentration of dye as well as C_t is concentration of dye at desired time t (as per min). Additionally, the amounts of half-life time ($t_{1/2}$) of the sonodegradation reactions were achieved by the equation in below (5):

$$t_{1/2} = \ln 2/k_{app} \quad (5)$$

The plots of $\ln(C_0/C_t)$ *versus* irradiation time (as per min) for the MB degradation reactions illustrate a straight line and the gained data shown in Fig. 9c and Table S2.† The values of

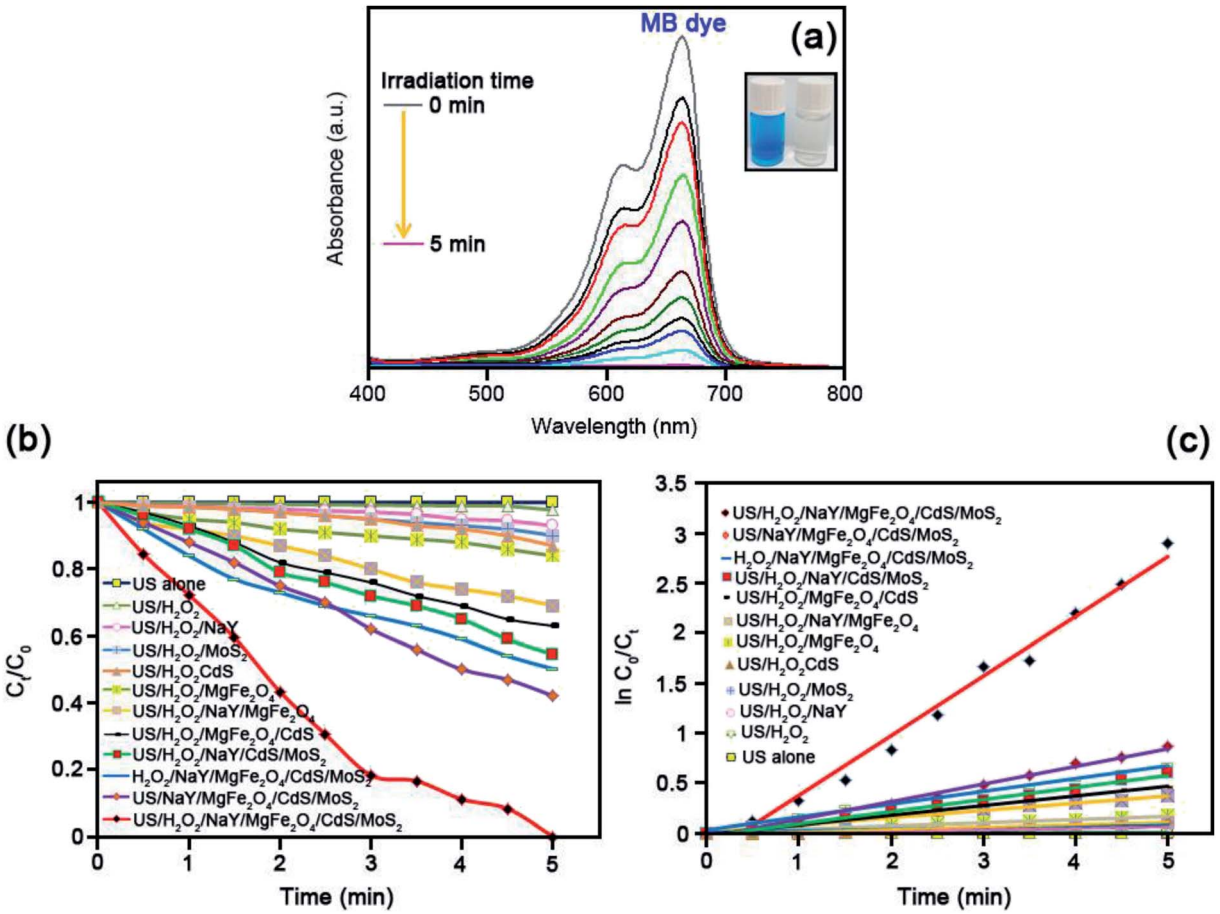

Fig. 9 (a) and (b) UV-vis absorption spectra changes of the sonocatalytic degradation of MB over the NaY/$MgFe_2O_4$/CdS NRs/MoS_2 NFs at different irradiation times. (c) First order kinetic plot of $\ln(C_0/C_t)$ *versus* irradiation time under the optimal conditions ($[MB]_o$: 25 mg L^{-1}, 50 mL, $[H_2O_2]_o$: 4 mM, 2 mL, NaY/$MgFe_2O_4$/CdS NRs/MoS_2 NFs dosage: 10 mg, US power: 100 W, pH = 7 at room temperature).

reaction rate constants were achieved *via* the slope of the straight line.

3.9.3. Process type. In order to precisely evaluate on the capability and functionality of each intended components in studying the sonodegradation process of the MB dye, multiple catalytic systems, involving US/H_2O_2/NaY/$MgFe_2O_4$/CdS/MoS_2, US/NaY/$MgFe_2O_4$/CdS/MoS_2, H_2O_2/NaY/$MgFe_2O_4$/CdS/MoS_2, US/H_2O_2/NaY/CdS/MoS_2, US/H_2O_2/$MgFe_2O_4$/CdS, US/H_2O_2/NaY/$MgFe_2O_4$, US/H_2O_2/$MgFe_2O_4$, US/H_2O_2/CdS, US/H_2O_2/MoS_2, US/H_2O_2/NaY, US/H_2O_2, and US alone were adopted as the gained outcomes are demonstrated in Fig. 9a–c and Table S2.† Regarding the outcomes, it was evident that the sonodegradation process efficiency increases in the following order of US alone < US/H_2O_2 (2.3%) < US/H_2O_2/NaY (7.1%) < US/H_2O_2/MoS_2 (9.9%) < US/H_2O_2/CdS (13.1%) < US/H_2O_2/$MgFe_2O_4$ (16%) < US/H_2O_2/NaY/$MgFe_2O_4$ (31.2%) < US/H_2O_2/$MgFe_2O_4$/CdS (36.9%) < US/H_2O_2/NaY/CdS/MoS_2 (45.5%) < H_2O_2/NaY/$MgFe_2O_4$/CdS/MoS_2 (49.8%) < US/NaY/$MgFe_2O_4$/CdS/MoS_2 (57.9%) < US/H_2O_2/NaY/$MgFe_2O_4$/CdS/MoS_2 (100%) with the apparent kinetic rate constants (k_{app}) of 0.000, 0.003, 0.012, 0.013, 0.025, 0.031, 0.072, 0.096, 0.119, 0.177, and 0.596 min^{-1}, respectively. From the above considerations, the US/H_2O_2/NaY/$MgFe_2O_4$/CdS/MoS_2 system illustrated the most effective result for the degradation of MB dye from water media, which is corresponded to the prevention of the electron–hole pairs recombination applying the linkage between the MoS_2, $MgFe_2O_4$, CdS and NaY zeolite. Additionally, *via* utilizing US irradiation along with H_2O_2 as a green and environmentally friendly oxidizing agent, the production of the $^{\bullet}OH$ free radicals remarkably increased. Eventually, the more the number of the formed $^{\bullet}OH$ free radicals leading to the enhancement sonodegradation performance of MB dye.

3.9.4. Effect of initial concentration of MB. The effect of initial MB concentration in the sonodegradation reactions utilizing the NaY/$MgFe_2O_4$/CdS NRs/MoS_2 NFs sonocatalyst was investigated *via* altering the concentration of MB dye from 25–45 mg L^{-1} respectively as the outcomes attained were reflected in Fig. 10a. From Fig. 10a, it was understood that the sonodegradation reaction rate tended to decrease as the initial dye concentration was more increased. A reason for this trend can be corresponded to the more occupies of available active sites of the sonocatalyst *via* the MB molecules, which can lead to reduce the catalytic performance. As well, the other possible reason for

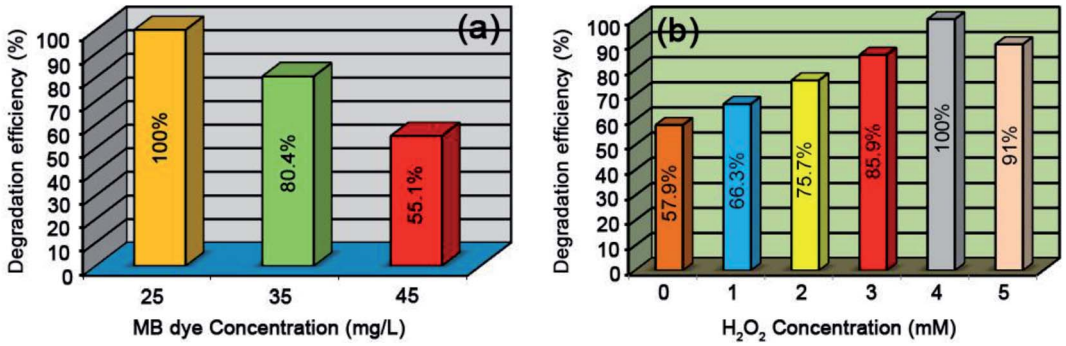

Fig. 10 The effects of: (a) initial MB concentrations and (b) initial H_2O_2 concentration on the sonocatalytic degradation of MB by the NaY/$MgFe_2O_4$/CdS NRs/MoS_2 NFs nanocomposite.

this phenomenon may be related to the remarkable absorption of US waves *via* the dye molecules in the reaction solution.

3.9.5. Effect of H_2O_2 concentration. In order to find the optimal H_2O_2 concentration for the sonodegradation of MB dye using the NaY/$MgFe_2O_4$/CdS NRs/MoS_2 NFs system, the H_2O_2 amounts were changed ranging from 1 to 5 mM, while the another analytical factors were remained constant. With respect to the achieved outcomes from Fig. 10b, approximately 57.9% of MB dye was eliminated in the absence of H_2O_2 oxidizing agent. However, after adding various H_2O_2 concentrations from 1–4 mM, the sonodegradation reaction rates were found to be 66.3% to 100%, respectively after 5 min of US irradiation. This trend can be explained by this fact that by increasing H_2O_2 concentration values, the $^{\bullet}OH$ radicals formation notable increased. Conversely, the degradation process efficiency decreased by increasing the appended hydrogen peroxide concentration higher than 4 mM, while can be due to the production of the further $^{\bullet}O_2H$ radicals with a lesser oxidation performance. Taking all this into account, the initial H_2O_2 concentration of 4 mM was considered as the optimal amount in studying the sonodegradation experiments.

3.9.6. Effect of organic dye type. To attain further insights into the NaY/$MgFe_2O_4$/CdS NRs/MoS_2 NFs activity, the sonocatalytic performance of this nanocomposite was assessed in the presence of two cationic and anionic dyes namely RhB and MO under the optimal conditions. Regarding the obtained results

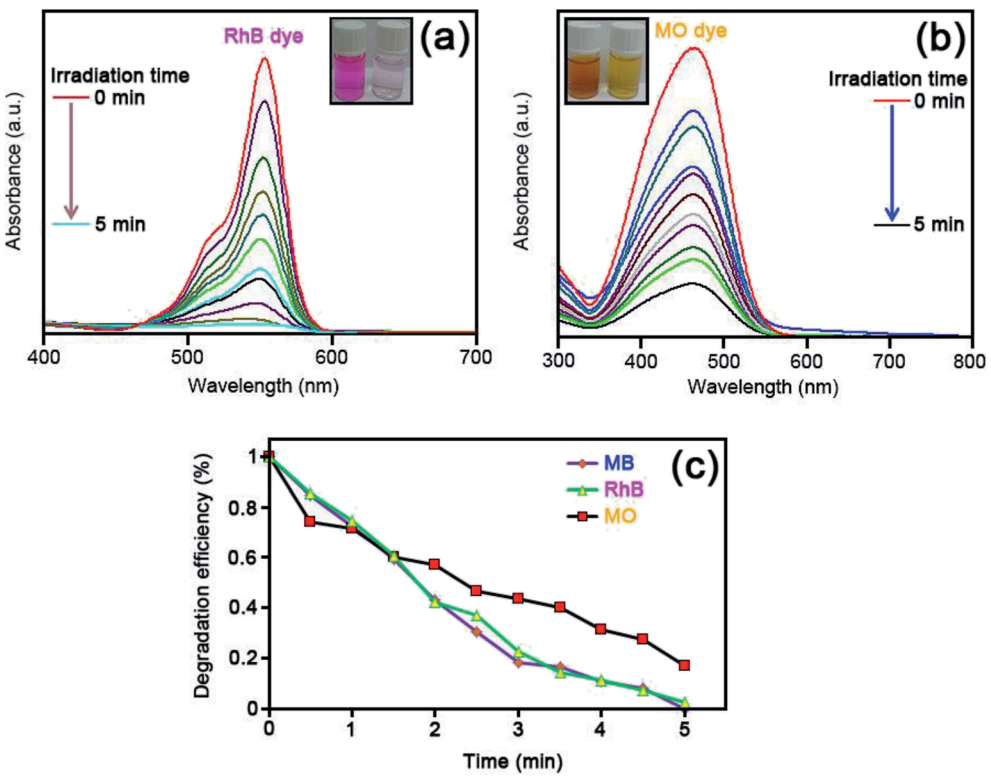

Fig. 11 UV-vis absorption spectra changes of: (a) RhB, and (b) MO organic dyes. (c) Plot of the degradation efficiency% *versus* the irradiation time in the presence of NaY/$MgFe_2O_4$/CdS NRs/MoS_2 NFs catalyst.

from Fig. 11a–c, the degradation process rates of RhB (λ_{max} = 554 nm) and MO (λ_{max} = 465 nm) were found to be 97.3% and 82.8% respectively after irradiation time of 10 min. These collected data clearly revealed that the multiple factors of organic dyes, including electric charges, structure, molecule sizes and more, can lead to the differences in the NaY/$MgFe_2O_4$/CdS NRs/MoS_2 NFs activity in their degradation process.

3.9.7. Effect of catalyst dosage. The effect of catalyst dosage on the sonodegradation process of MB dye was obtained with the optimal nanocomposite under the same conditions. Fig. 12a illustrates the NaY/$MgFe_2O_4$/CdS NRs/MoS_2 NFs sonocatalytic performance at various catalyst dosages of 5, 10, 25, 50, 75 and 100 mg, respectively. As can be seen in Fig. 12a, it was clearly found that the sonodegradation reaction efficiency increases up to 10 mg and subsequently a decreasing for 75 mg dosage. This phenomenon can be explained due to the decrease of its available active sites to produce the free $^{\bullet}OH$ radicals. Also, other reason for this behavior can be related to the reaction solution becomes turbid because of the suspended solid particles, which leads to the decrease of transmission of US irradiation into the system. Thus, the amount of 10 mg of the NaY/$MgFe_2O_4$/CdS NRs/MoS_2 NFs nanocomposite is fixed as the optimal dosage of the catalyst to investigate the sonodegradation process of MB dye under US irradiation.

3.9.8. Effect of US power. The ultrasonic device power is introduced as other remarkable practical parameter in evaluating the MB sonodegradation reactions activity. Fig. 12b demonstrates that the sonodegradation rate of MB dye (25 mg L^{-1}) using the NaY/$MgFe_2O_4$/CdS NRs/MoS_2 NFs nanocomposite was increased *via* increasing the US power from 40 W to 100 W within 5 min of irradiation time. This outcome can be due to the increase in the number of cavitation, which can lead to the introduction of the more active $^{\bullet}OH$ radicals in the reaction solution and eventually the promotes the MB sonodegradation yield.

3.9.9. Stability and recyclability of the NaY/$MgFe_2O_4$/CdS NRs/MoS_2 NFs. One of the most important advantages of utilizing the heterogeneous catalysts in the effluents remediation is their capability for recycle multiple times. Therefore, the recyclability and stability of the as-fabricated NaY/$MgFe_2O_4$/CdS NRs/MoS_2 NFs nanocomposite sonocatalyst was implemented after immersing in a water–ethanol solution. The obtained outcomes depicted that sonodegradation rate only slightly decreased even after four sequential runs up to 94.5% of recycle, revealing that the NaY/$MgFe_2O_4$/CdS NRs/MoS_2 NFs sonocatalyst has a high structural stability (see Fig. 12c). On the other hand, the nature of the reused sonocatalyst was also investigated. As can be represented in Fig. S2a–c,† the FTIR, FESEM and EDAX spectra of the reused NaY/$MgFe_2O_4$/CdS NRs/MoS_2 NFs sonocatalyst should no remarkable change between the recovered sonocatalyst and the fresh after four times. Thereupon, the abovementioned results clearly verified that the NaY/$MgFe_2O_4$/CdS NRs/MoS_2 NFs nanocomposite structure is stable against the sonodegradation processes as a particular advantage for its experimental approach.

3.9.10. Comparison with other catalytic systems. In order to compare the activity of the as-manufactured NaY/$MgFe_2O_4$/CdS NRs/MoS_2 NFs nanocomposite on the degradation of organic dyes, the applicability of this nanocomposite *versus* the other catalysts were evaluated as the achieved data were collected in Table S3.†[6,10–12,14,16,44,45] According to the presented outcomes, it was clarified that the NaY/$MgFe_2O_4$/CdS NRs/MoS_2 NFs nanocomposite has a significant performance regarding the initial dye concentration, irradiation time, sonocatalyst dosage, and reaction yield against the other catalysts reported.

3.9.11. Plausible sonocatalytic mechanism of the US/H_2O_2/NaY/$MgFe_2O_4$/CdS NRs/MoS_2 NFs system. The valence band

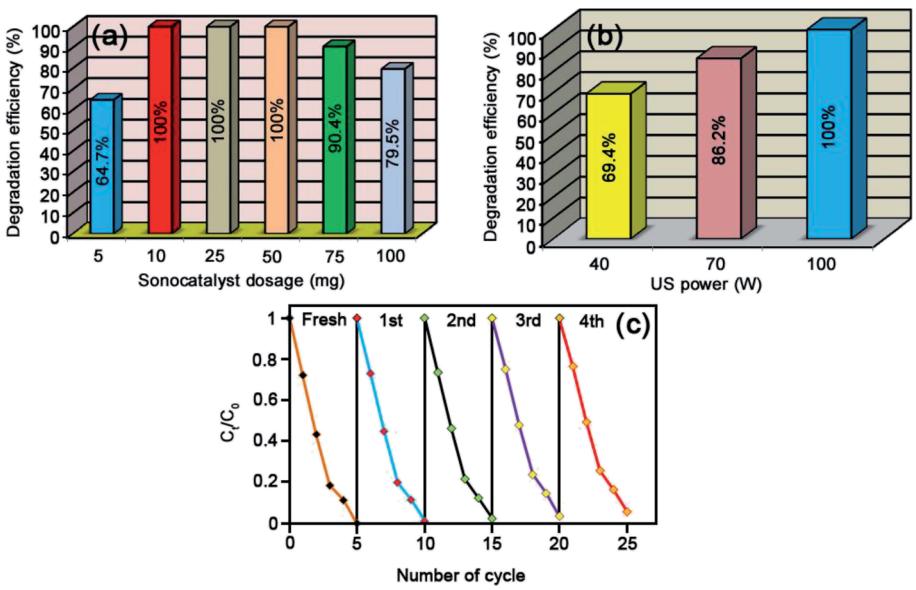

Fig. 12 The effects of: (a) NaY/$MgFe_2O_4$/CdS NRs/MoS_2 NFs dosage, (b) US power and (c) recyclability of the NaY/$MgFe_2O_4$/CdS NRs/MoS_2 NFs catalyst on the sonocatalytic degradation of MB.

(E_{VB}) and conduction band (E_{CB}) energies of the bare MoS_2 NFs, bare CdS NRs and bare $MgFe_2O_4$ were determined by the atom's Mulliken electronegativity theory, which is represented regarding the equations in below (eqn (6) and (7)):

$$E_{VB} = \chi - E^e + \frac{E_g}{2} \quad (6)$$

$$E_{CB} = E_{VB} - E_g \quad (7)$$

In the above equations, E_{VB} and E_{CB} symbols are the VB and the CB energies respectively, E^e is the energy of free electrons on the hydrogen scale (4.5 eV), and χ factor is the absolute electronegativity of the enumerated semiconductors. Based on the aforementioned equations, the amounts of E_{VB} and E_{CB} energies of the bare CdS were acquired to be 1.88 eV and −0.52 eV, respectively. Moreover, E_{VB} and E_{CB} energies of the bare MoS_2 were found to be 1.75 eV and −0.15 eV, whereas the energies for the bare $MgFe_2O_4$ were calculated to be 2.13 eV and 0.49 eV, respectively.

Regarding the acquired results herein, a plausible degradation mechanism for the US/H_2O_2/NaY/$MgFe_2O_4$/CdS/MoS_2 system is suggested in detail. Overall, the sonodegradation reaction contains sonoluminescence, hot spots and oxygen atom escape contributed. The sonoluminescence is well-known as a process during which the US cavitation produces the visible light with a wide wavelength. Furthermore, the production of hot spots leads to increase the pressure and temperature of the reaction solution up to 100 MPa and 5000 K respectively inside the cavitation bubbles which cause splits hydrogen peroxide and oxygen molecules over the surface of catalyst to form the $^{\bullet}OH$ free radicals and superoxide radical anions ($^{\bullet}O_2^-$). After absorbing the visible light and heat *via* the NaY/$MgFe_2O_4$/CdS NRs/MoS_2 NFs surface, MoS_2, $MgFe_2O_4$ and CdS semiconductors were excited and then h^+–e^- pairs were generated in their conduction and conduction bands. Because of CB energy of the CdS ($E_{CB} = -0.52$ eV) compared with the CB energies of the MoS_2 ($E_{CB} = -0.15$ eV) and $MgFe_2O_4$ ($E_{CB} = 0.49$ eV) is more negative, the produced electrons on the e_{CB}^- of CdS can easily transfer to the e_{CB}^- of MoS_2 and e_{CB}^- of $MgFe_2O_4$, respectively. Meantime, Because of VB energies of the $MgFe_2O_4$ ($E_{VB} = 2.13$ eV) and CdS ($E_{VB} = 1.88$ eV) are more positive that of VB energy of MoS_2 ($E_{VB} = 1.75$ eV), the formed holes can be jumped in the opposite directions from h_{VB}^+ of CdS and h_{VB}^+ of $MgFe_2O_4$ to the h_{VB}^+ of MoS_2. Additionally, it worth nothing that since the NaY zeolite has not good electronic conductivity, thus it can be considered as an excellent electron acceptor–donor and transporter. Considering the aforementioned explanations, the available electrons on the $MgFe_2O_4$ (e_{CB}^-) can be jumped over the surface of NaY zeolite. In the next step, the electrons collected within the zeolite surface can react with H_2O_2 and O_2 molecules to generate $^{\bullet}OH$ free radicals and superoxide radical anions ($^{\bullet}O_2^-$). Simultaneously, the gathered holes on the MoS_2 (h_{VB}^+) can react with OH^- and H_2O molecules to produce the more $^{\bullet}OH$ free radicals. Eventually, the produced reactive oxygen species can oxidize the organic dye molecules adsorbed on the surface of NaY/$MgFe_2O_4$/CdS NRs/MoS_2 NFs nanocomposite catalyst and resulting in the dyes decomposition and the formation of harmless products of CO_2, H_2O, NO_3^-, NH_4^+, *etc.* The steps include on the plausible mechanism of the sonodegradation process using the NaY/$MgFe_2O_4$/CdS NRs/MoS_2 NFs catalyst have been summarized according to the eqn (8)–(17) and also delineated as a pictorial illustration in Fig. 13.

$$\text{Ultrasonic irradiation} \rightarrow \text{heat} + \text{light} \quad (8)$$

$$\text{NaY/MgFe}_2\text{O}_4\text{/CdS/MoS}_2 + \text{heat and/or light} \rightarrow \text{NaY/[MgFe}_2\text{O}_4\text{/CdS/MoS}_2\text{]}^* \quad (9)$$

$$[\text{MgFe}_2\text{O}_4\text{/CdS/MoS}_2]^* \rightarrow [\text{MgFe}_2\text{O}_4\text{/CdS/MoS}_2]\ (e_{CB}^- + h_{VB}^+) \quad (10)$$

$$(e_{CB}^-)\ \text{CdS} + \text{MoS}_2 \rightarrow \text{CdS} + (e_{CB}^-)\ \text{MoS}_2 \quad (11)$$

$$(e_{CB}^-)\ \text{MoS}_2 + \text{MgFe}_2\text{O}_4 \rightarrow \text{MoS}_2 + (e_{CB}^-)\ \text{MgFe}_2\text{O}_4 \quad (12)$$

$$(e_{CB}^-)\ \text{MgFe}_2\text{O}_4 + \text{NaY} \rightarrow \text{MgFe}_2\text{O}_4 + (e^-)\ \text{NaY} \quad (13)$$

$$(h_{VB}^+)\ \text{CdS} + (h_{VB}^+)\ \text{MgFe}_2\text{O}_4 + \text{MoS}_2 \rightarrow \text{CdS} + \text{MgFe}_2\text{O}_4 + (h_{VB}^+)\ \text{MoS}_2 \quad (14)$$

$$^{\bullet}OH + OH^- + {}^{\bullet}O_2^- + \text{NaY} \rightarrow (e^-)\ \text{NaY} + H_2O_2/O_2 \quad (15)$$

$$(h_{VB}^+)\ \text{MoS}_2 + H_2O \text{ and/or } OH^- \rightarrow \text{MoS}_2 + {}^{\bullet}OH \quad (16)$$

$$^{\bullet}OH/{}^{\bullet}O_2^- + \text{dyes} \rightarrow CO_2, H_2O, NO_3^-, NH_4^+ \text{ and more} \quad (17)$$

3.9.12. The plausible sonocatalytic mechanism evidences. In order to confirm the sonodegradation process mechanism, the photoluminescence (PL) and scavenger tests were performed. The photoluminescence (PL) is a suitable analysis to study the separation and migration efficiency of the sonoexcited carriers between the $MgFe_2O_4$, MoS_2 and CdS semiconductors. The PL spectra of the bare CdS NRs (Fig. 14a(i)), $MgFe_2O_4$/CdS

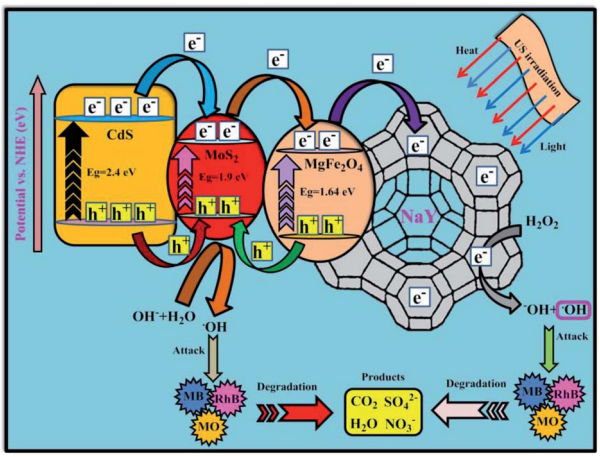

Fig. 13 A plausible mechanism for the sonodegradation reaction of organic dyes applying the US/H_2O_2/NaY/$MgFe_2O_4$/CdS/MoS_2 system from water media under US irradiation.

NRs (Fig. 14a(ii)), and NaY/$MgFe_2O_4$/CdS NRs/MoS_2 NFs (Fig. 14a(iii)) have been evidenced in Fig. 14a. Regarding the presented outcomes, it was observed that the bare CdS NRs indicate the PL spectrum with a high intensity near 540 nm, which is allocated to the fast recombination of hole–electron (h^+–e^-) pairs. However, upon coupling the CdS with $MgFe_2O_4$ and MoS_2, the intended emission peak intensity noteworthy reduced, affirming that the as-manufactured nanocomposites has a high potential for the separation of the sonogenerated e^-–h^+ pairs. According to the above explanations, it was concluded that the generation of the $MgFe_2O_4$/CdS NRs/MoS_2 NFs heterojunction can help to inhibit e^-–h^+ recombination owing to the influence of two co-catalytic of the MoS_2 and $MgFe_2O_4$ semiconductors, which increases the lifetime of charge carriers, and therefore is favorable for the enhancement of sonocatalytic activity.

On the other hand, owing to the peculiar role of reactive oxygen species through the sonodegradation processes, the various types of radical scavengers were added into the understudy working solution. For this purpose, the three reagents, including benzoquinone (BQ), *tert*-butyl alcohol (*t*-BuOH) and ethylenediaminetetraacetate (EDTA) were selected as $^{\bullet}O_2^-$, $^{\bullet}OH$ and h^+ radical scavengers, respectively. With respect to the presented analytical information from Fig. 14b, it was observed that the addition of EDTA and BQ revealed no remarkable decrease on the MB dye sonodegradation efficiency. This outcome corroborated that h^+ and $^{\bullet}O_2^-$ scavengers don't play a main role on studying the sonodegradation reactions. On the contrary, *t*-BuOH appended into working solution exhibited a quickly decrease on the sonodegradation performance, which clearly proved the notable role of $^{\bullet}OH$ radicals in the MB degradation processes. Regarding the gathered outcomes, the decrease of the sonodegradation activity using the scavengers provides the following order: *t*-BuOH > EDTA > BQ.

Additionally, the production of $^{\bullet}OH$ radicals on the NaY/$MgFe_2O_4$/CdS NRs/MoS_2 NFs surface was further confirmed *via* the PL analysis applying terephthalic acid (TPA) as a probe molecule. The non-fluorescent TPA reacts with $^{\bullet}OH$ radicals to produce a fluorescent product namely 2-hydroxy terephthalic acid (h-TPA), which can be monitored using the PL analysis to evaluate the production of $^{\bullet}OH$ radicals in the reaction solution. Fig. 14c reveals the change in the PL intensity of h-TPA under US irradiation of TPA solution for 5 min in the presence of the NaY/$MgFe_2O_4$/CdS NRs/MoS_2 NFs catalyst. As can be seen in Fig. 14c, the PL intensity gradually increases by increasing the irradiation time at 420 nm. Based on the obtained results, it can be found that $^{\bullet}OH$ radicals are the main reactive species included in the MB dye degradation in the presence of the NaY/$MgFe_2O_4$/CdS NRs/MoS_2 NFs catalyst.

4. Conclusion

In conclusion, the present research was carried out to ultrasonic-assisted solvothermally fabricate the magnetically separable NaY zeolite/$MgFe_2O_4$/CdS NRs/MoS_2 NFs nanocomposite for sonocatalysis degradation of toxic organic dyes.

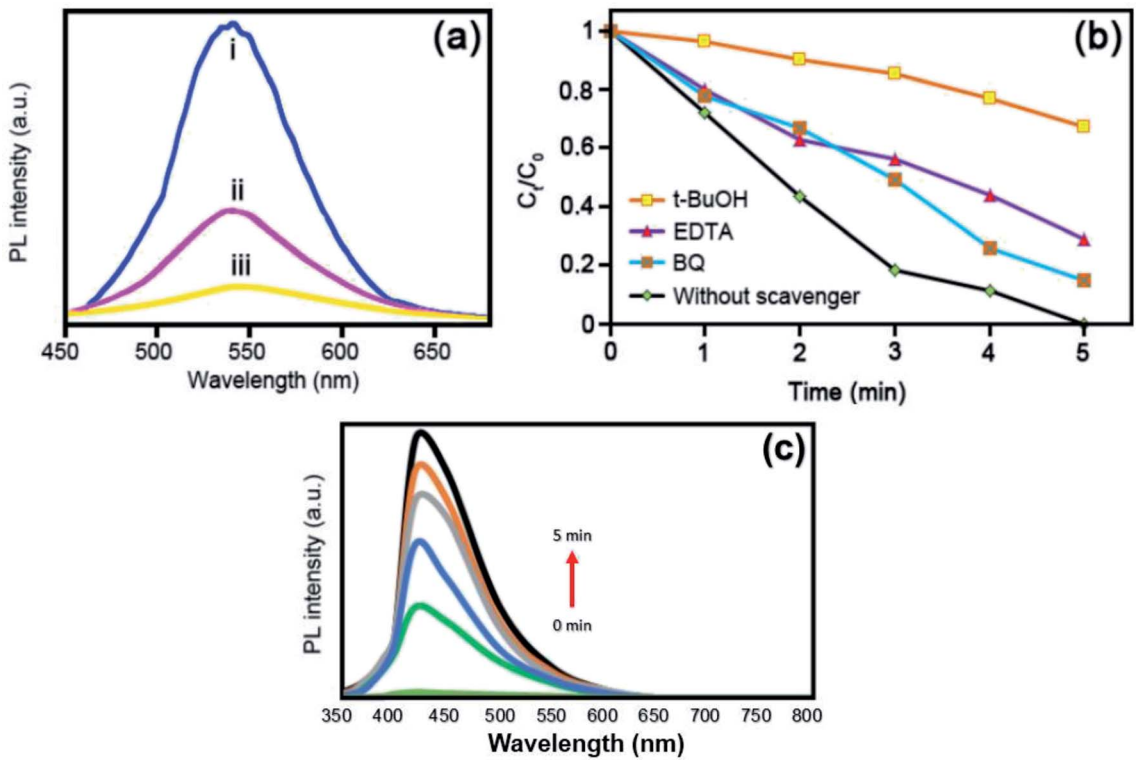

Fig. 14 (a) PL emission spectra of: (i) bare CdS, (ii) $MgFe_2O_4$/CdS and (iii) NaY/$MgFe_2O_4$/CdS/MoS_2, (b) the effect of scavenger type over the sonodegradation reaction of MB utilizing the NaY/$MgFe_2O_4$/CdS/MoS_2 nanocomposite, and (c) PL emission spectra of TPA in the presence of NaY/$MgFe_2O_4$/CdS/MoS_2 sonocatalyst under US irradiation.

The gained outcomes of FESEM, EDAX, FTIR, XRD, TEM, AFM, VSM, N_2-BET, UV-vis DRS, and PL analyses obviously affirmed the successful fabrication of NaY/$MgFe_2O_4$/CdS NRs/MoS_2 NFs sonocatalyst. The activity of the as-fabricated NaY/$MgFe_2O_4$/CdS NRs/MoS_2 NFs nanocomposite was evaluated for the degradation of methylene blue (MB), rhodamine B (RhB) and methyl orange (MO) from water solutions. The experimental outcomes demonstrated that sonodegradation reactions kinetic of MB could be described applying the first-order kinetic model. The apparent rate constant (k_{app}) and half-life time ($t_{1/2}$) obtained for the sonodegradation reaction of MB dye *via* the US/H_2O_2/NaY/$MgFe_2O_4$/CdS/MoS_2 system were measured to be 1.162 min and 0.596 min^{-1}, respectively. The effects of several practical factors on the catalytic performance of this nanocomposite, including irradiation time, process type, initial MB concentration, H_2O_2 concentration, catalyst dosage, organic dye type, US power, and scavenger type were thoroughly surveyed. The trapping experiments displayed that hydroxyl radicals ($^{\bullet}OH$) constitute the main reactive oxidizing species on the sonodegradation reaction of organic dyes. The recyclability of the as-fabricated NaY/$MgFe_2O_4$/CdS NRs/MoS_2 NFs sonocatalyst was conducted in multiple sequential runs, and a loss of less than 6% was obtained in the sonodegradation efficiency after four runs. In addition, owing to the excellent degradation performance, this nanocomposite can be a recommendable choice for the remediation of hazardous organic sewages in the future.

Conflicts of interest

There are no conflicts to declare.

Acknowledgements

The financial support of the Laboratory at the Lorestan University, Khorramabad, Iran is gratefully acknowledged.

References

1 M. S. Hossain, M. A. Z. Chowdhury, M. K. Pramanik, M. A. Rahman, A. N. M. Fakhruddin and M. K. Alam, *Appl. Water Sci.*, 2015, **5**, 171–179.
2 M. Sadeghi, S. Farhadi and A. Zabardasti, *RSC Adv.*, 2020, **10**, 10082–10096.
3 R. Zhao, Y. Wang, X. Li, B. Sun and C. Wang, *ACS Appl. Mater. Interfaces*, 2015, **7**, 26649–26657.
4 A. A. Hoseini, S. Farhadi, A. Zabardasti and F. Siadatnasab, *RSC Adv.*, 2019, **9**, 24489–24504.
5 A. Hassani, P. Eghbali, A. Ekicibil and Ö. Metin, *J. Magn. Magn. Mater.*, 2018, **456**, 400–412.
6 F. Siadatnasab, S. Farhadi and A. Khataee, *Ultrason. Sonochem.*, 2018, **44**, 359–367.
7 S. Chakma and V. S. Moholkar, *J. Taiwan Inst. Chem. Eng.*, 2016, **60**, 469–478.
8 M. Sadeghi, S. Farhadi and A. Zabardasti, *New J. Chem.*, 2020, **44**, 8386–8401.
9 Y. L. Pang and A. Z. Abdullah, *Ultrason. Sonochem.*, 2012, **19**, 642–651.
10 F. Siadatnasab, S. Farhadi, A. A. Hoseini and M. Sillanpää, *New J. Chem.*, 2020, **44**, 16234–16245.
11 M. Zhou, H. Yang, T. Xian, R. Li, H. Zhang and X. Wang, *J. Hazard. Mater.*, 2015, **289**, 149–157.
12 S. Farhadi and F. Siadatnasab, *Desalin. Water Treat.*, 2017, **66**, 299–308.
13 S. Farhadi and F. Siadatnasab, *Mater. Res. Bull.*, 2016, **83**, 345–353.
14 M. Chauhan, N. Kaur, P. Bansal, R. Kumar, S. Srinivasan and G. R. Chaudhary, *J. Nanomater.*, 2020, 1–15, DOI: 10.1155/2020/6123178.
15 P. Nuengmatcha, S. Chanthai, R. Mahachai and W.-C. Oh, *Dyes Pigm.*, 2016, **134**, 487–497.
16 S. Sajjadi, A. Khataee and M. Kamali, *Ultrason. Sonochem.*, 2017, **39**, 676–685.
17 R. K. Chava, J. Y. Do and M. Kang, *Appl. Surf. Sci.*, 2018, **433**, 240–248.
18 S. K. Tang, T. T. Teng, A. F. M. Alkarkhi and Z. Li, *APCBEE Procedia*, 2012, **1**, 110–115.
19 Y. Min, K. Zhang, Y. C. Chen and Y. G. Zhang, *Ultrason. Sonochem.*, 2012, **19**, 883–889.
20 A. R. Bagheri, M. Ghaedi, A. Asfaram, R. Jannesar and A. Goudarzi, *Ultrason. Sonochem.*, 2017, **35**, 112–123.
21 P. Gao, J. Liu, D. D. Sun and W. Ng, *J. Hazard. Mater.*, 2013, **250**, 412–420.
22 W. Jiang, Y. Liu, R. Zong, Z. Li, W. Yao and Y. Zhu, *J. Mater. Chem. A*, 2015, **3**, 18406–18412.
23 G. Kartopu, D. Turkay, C. Ozcan, W. Hadibrata, P. Aurang, S. Yerci, H. E. Unalan, V. Barrioz, Y. Qu, L. Bowen, A. K. Gürlek, P. Maiello, R. Turan and S. J. C. Irvine, *Sol. Energy Mater. Sol. Cells*, 2018, **176**, 100–108.
24 I. M. Dharmadasa, P. A. Bingham, O. K. Echendu, H. I. Salim, T. Druffel, R. Dharmadasa, G. U. Sumanasekera, R. R. Dharmasena, M. B. Dergacheva, K. A. Mit, K. A. Urazov, L. Bowen, M. Walls and A. Abbas, *Coatings*, 2014, **4**, 380–415.
25 X. D. Li, S. Q. Wu and Z. Z. Zhu, *J. Mater. Chem. C*, 2015, **3**, 9403–9411.
26 M. hong Wu, L. Li, N. Liu, D.-j. Wang, Y.-c. Xue and Li. Tang, *Process Saf. Environ. Protect.*, 2018, **118**, 40–58.
27 A. Ramadoss, T. Kim, G. Shik Kim and S. J. Kim, *New J. Chem.*, 2014, **38**, 2379–2385.
28 W. Choi, N. Choudhary, G. Hee Han, J. Park, D. Akinwande and Y. H. Lee, *Mater. Today*, 2017, **20**, 116–130.
29 W. Zhang, P. Zhang, Z. Su and G. Wei, *Nanoscale*, 2015, **7**, 18364–18378.
30 J. C. Hern and K. F. W. Y. Momade, *J. Sol-Gel Sci. Technol.*, 2013, **65**, 189–194.
31 M. Shahid, L. Jingling, Z. Ali, I. Shakir, M. F. Warsi, R. Parveen and M. Nadeem, *Mater. Chem. Phys.*, 2013, **139**, 566–571.
32 H. Zhou, L. Hu, J. Wan, R. Yang, X. Yu, H. Li, J. Chen, L. Wang and X. Lu, *Chem. Eng. J.*, 2016, **284**, 54–60.
33 C. J. Jia, Y. Liu, M. Schwickardi, C. Weidenthaler, B. Spliethoff, W. Schmidt and F. Schuth, *Appl. Catal. Gen.*, 2010, **386**, 94–100.

34 A. G. Abraham, A. Manikandan and E. Manikandan, *J. Magn. Magn. Mater.*, 2018, **452**, 380–388.
35 D. Kang, X. Yu, M. Ge and W. Song, *Microporous Mesoporous Mater.*, 2015, **207**, 170–178.
36 V. Srivastava, Y. C. Sharma and M. Sillanpää, *Appl. Surf. Sci.*, 2015, **338**, 42–54.
37 M. Kaur, N. Kaur, K. Jeet and P. Kaur, *Ceram. Int.*, 2015, **41**, 13739–13750.
38 J. Patil, D. Nadargi, I. S. Mulla and S. S. Suryavanshi, *Mater. Lett.*, 2018, **213**, 27–30.
39 S. Kanagesan, M. Hashim, S. Tamilselvan, N. B. Alitheen, I. Ismail and G. Bahmanrokh, *J. Nanomater.*, 2013, **2013**, 865024.
40 M. Sadeghi, S. Yekta, H. Ghaedi and E. Babanezhad, *Mater. Chem. Phys.*, 2017, **197**, 113–122.
41 M. Dehghani, A. Tadjarodi and S. Chamani, *ACS Omega*, 2019, **4**, 10640–10648.
42 M. Sadeghi, S. Yekta, D. Mirzaei, A. Zabardasti and S. Farhadi, *J. Inclusion Phenom. Macrocycl. Chem.*, 2019, **93**, 215–227.
43 H. Ramezani, S. N. Azizi and S. R. Hosseini, *Sensor. Actuator. B Chem.*, 2017, **248**, 571–579.
44 F. Li, J. Wu, Q. Qin, Z. Li and X. Huang, *Powder Technol.*, 2010, **198**, 267–274.
45 A. Mokhtari Andani, T. Tabatabaie, S. Farhadi and B. Ramavandi, *RSC Adv.*, 2020, **10**, 32845–32855.